Monthly Notices
of the
ROYAL ASTRONOMICAL SOCIETY

MNRAS **445,** 604–613 (2014) doi:10.1093/mnras/stu1765

Emission mechanism of *GeV-quiet* soft gamma-ray pulsars: a case for peculiar geometry?

Y. Wang, C. W. Ng, J. Takata,★ Gene C. K. Leung and K. S. Cheng

Department of Physics, University of Hong Kong, Pokfulam Road, Hong Kong

Accepted 2014 August 23. Received 2014 August 15; in original form 2014 July 18

ABSTRACT

There is a growing new class of young spin-down powered pulsars called GeV-quiet soft gamma-ray pulsar; (1) spectral turnover appears around 10 MeV, (2) the X-ray spectra of below 20 keV can be described by power law with a photon index of around 1.2 and (3) the light curve in X-ray/soft gamma-ray bands shows single broad pulse. Their emission properties are distinct from the normal gamma-ray pulsars, for which the spectral peak in νF_ν appears in GeV energy bands and the X-ray/gamma-ray light curves show sharp and double (or more) peaks. In this paper, we discuss that X-ray/soft gamma-ray emissions of the GeV-quiet soft gamma-ray pulsars are caused by the synchrotron radiation of the electron/positron pairs, which are created by the magnetic pair-creation process near the stellar surface. In our model, the viewing geometry is a crucial factor to discriminate between the normal gamma-ray pulsars and soft gamma-ray pulsars. Our model suggests that the difference between the magnetic inclination angle (α) and the Earth viewing angle (β) of the soft gamma-ray pulsars is small, so that the synchrotron emissions from the high magnetic field region around the polar cap region dominate in the observed emissions. Furthermore, the inclination angle of the soft gamma-ray pulsar is relatively small, $\alpha \leq 30^\circ$, and our line of sight is out of the gamma-ray beam emitted via the curvature radiation process in the outer gap. We also analyse the six year *Fermi* data for four soft gamma-ray pulsars to determine the upper limit of the GeV flux.

Key words: radiation mechanisms: non-thermal – stars: neutron – pulsars: general – gamma-rays: stars.

1 INTRODUCTION

The *Fermi* gamma-ray telescope has discovered about 150 gamma-ray pulsars.[1] The *Fermi* revealed that the pulsars with high spin-down power emit the GeV gamma-rays and the typical gamma-ray spectra are described by the single power-law plus exponential cut-off function with a cut-off energy ∼GeV. It is now widely accepted that the GeV gamma-ray emission region locates in outer magnetosphere near the light cylinder, where the corotation speed with the pulsar becomes the speed of light (Aliu et al. 2008; Abdo et al. 2010a).

The *soft gamma-ray pulsar* is a growing new class of young spin-down powered pulsars that are observed in the non-thermal X-rays and soft gamma-ray bands (Kuiper & Hermsen 2013). These soft gamma-ray pulsars are divided into two groups, that is, GeV-loud (e.g. Crab and Vela pulsars) and GeV-quiet. Currently, six GeV-quiet soft gamma-ray pulsars (hereafter, GeV-quiet SGPSRs) have been known: PSRs B1509−58, J1617−5055, J1811−1925, J1838−0655, J1846−02658 and J1930+1852. Fig. 1 summarizes the spin-down power, characteristic age and spectral characteristics of the radio pulsars (small dots), *Fermi*-Large Area Telescope (LAT) pulsars (filled boxes) and GeV-quiet SGPSRs (filled circles). We can see in Fig. 1 that GeV-quiet SGPSRs have a relatively large spin-down power and small characteristic age. Furthermore, we find in Fig. 1 that the spectral properties of GeV-quiet SGPSRs are distinct from those of the *Fermi*-LAT pulsars, that is, the weaker gamma-ray emissions but a stronger X-ray emissions comparing with the *Fermi*-LAT pulsars. In fact, all of GeV-quiet SGPSRs show (1) no GeV emissions and (2) a single broad light curve in X-ray/soft gamma-ray bands. The original one, PSR B1509−58, was first recognized as the Crab-type pulsar (Ulmer et al. 1993), since the spectral peak appears in ∼1 MeV energy, which resembles the spectrum of the Crab pulsar (Kuiper et al. 2001). Unlike the Crab pulsar, however, the offset of radio/X-ray peak phases is fairly large (Abdo et al. 2010b). Moreover, the *Fermi* revealed that PSR B1509−58 is not bright in GeV gamma-ray bands (Abdo et al. 2010b), which is incompatible with the spectrum of the Crab pulsar, suggesting that the X-ray/gamma-ray emission mechanism of the PSR B1509−58 is different from that of the Crab

★ E-mail: takata@hku.hk

[1] For updated list, see https://confluence.slac.stanford.edu/display/GLAMCOG/Public+List+of+LAT-Detected+Gamma-Ray+Pulsars

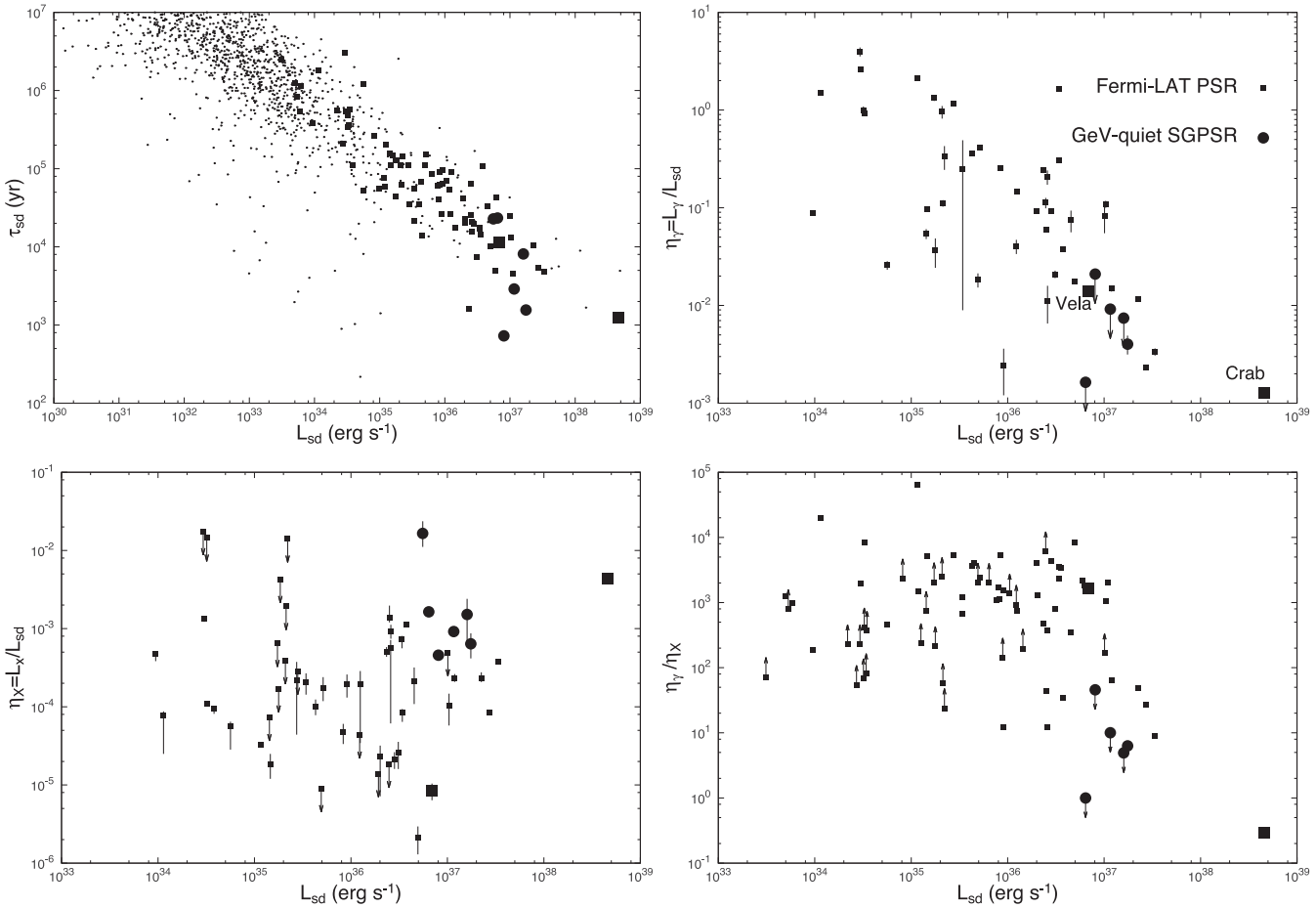

Figure 1. Characteristics of the canonical pulsars. Small dots, filled boxes and filled circles show the radio pulsars, *Fermi*-LAT pulsars and GeV-quiet SGPSRs, respectively. The large filled boxes located at $L_{sd} = 7 \times 10^{36}$ and 4.6×10^{38} erg s^{-1} correspond to the Vela and Crab pulsars, respectively. Top left: spin-down power versus the characteristic age. Top right: spin-down power versus gamma-ray efficiency. $L_\gamma = 4\pi D^2 F_\gamma$, where D is the distance and F_γ is the observed flux above 100 MeV. Bottom left: spin-down power versus X-ray efficiency. $L_X = 4\pi D^2 F_X$, where F_X is the observed X-ray flux below 10 keV. Bottom right: spin-down power versus η_γ / η_X. We extensively used the ATNF pulsar catalogue (Manchester et al. 2005) and the *Fermi* second catalogue of the pulsars (Abdo et al. 2013). We referred the observed X-ray flux of GeV-quiet SGPSRs from Becker & Aschenbach (2002) for J1617−5055, Torii et al. (1997) for J1811−1925, Lin et al. (2009) for J1838−0655, Gotthelf et al. (2000) for J1846−0258 and Camilo et al. (2002) for J1930+1852, respectively.

pulsar. In addition to PSR B1509−58, PSRs J1617−5055 (Torii et al. 1998), J1811−1925 (Torii et al. 1997), J1838−0655 (Lin et al. 2009), J1846−0258 (Gotthelf et al. 2000) and J1930+1852 (Camilo et al. 2002) are classified as GeV-quiet SGPSRs. Except for PSR J1617−5055, all of the SGPSRs are found in the centre of supernova remnants (SNR).

The formation of GeV-quiet soft gamma-ray spectra has not been conclusive yet. Zhang & Cheng (2000) discussed X-ray/gamma-ray emissions from PSR B1509−58 within a framework of the outer gap model and considered that PSR 1509−58 is the Crab-like pulsar, that is, the X-ray/gamma-ray emissions are created by the synchrotron radiation and inverse-Compton emissions of the electron and positron pairs created in the outer magnetosphere. The calculated overall spectrum qualitatively agrees with the multiwavelength data. However, the light cylinder radius of PSR B1509−69 is so large as to make it very difficult to attenuate all of the GeV curvature photons emitted from the outer gap, which may be inconsistent with no detection of GeV gamma-rays by *Fermi*.

Harding, Baring & Gonthier (1997) proposed operation of the photon-splitting process for the formation of the soft gamma-ray spectrum of PSR B1509−58, whose spin-down dipole magnetic field is $B_s \sim 2 \times 10^{13}$ G. They argued that as the stellar magnetic field approaches the critical value, $B_c \sim 4.4 \times 10^{13}$ G, the magnetic photon-splitting process plays an important role as attenuation of the gamma-rays emitted in the polar cap region. They discussed that the photon-splitting and pair-creation cascade process can explain the position of the spectral peak ∼10 MeV of PSR B1509−58. However, this model will not explain the soft gamma-ray spectra of PSRs J1617−5055 and J1811−1925, whose inferred magnetic fields are only $B_s \sim 3 \times 10^{12}$ and 2×10^{12} G, respectively, which are the typical values of the canonical gamma-ray pulsars.

Wang, Takata & Cheng (2013) proposed a new model for PSR B1509−58 in the framework of the outer gap accelerator model (Takata, Wang & Cheng 2010; Wang, Takata & Cheng 2010). They discussed that the Earth viewing angle measured from the rotation axis is smaller than (or close to) the inclination angle of the magnetic axis. In such a small viewing angle, the outward GeV emissions, which creates the observed spectra of the *Fermi*-LAT pulsars, are missed by the observer, while the inward emissions contribute to the observed emissions. Wang et al. (2013) argued furthermore that the magnetic pair-creation cascade initiated by the inward 0.1–1 GeV emissions near the stellar surface eventually produces the soft

Table 1. GeV-quiet SGPSRs. The second (P), third (L_{sd}) and fourth (B_s) columns are rotation period, spin-down power and surface dipole magnetic field, respectively. The fifth (D) is the distance to the source and is used to estimate the observed luminosity in Fig. 1. The sixth (α), seven (β) and eight (f_{gap}) are the magnetic inclination angle, Earth viewing angle and the fractional gap thickness, respectively, inferred from the fitting of the observations. The fitting result for PSR B1509−68 was taken from Wang et al. (2013). We did not fit PSR J1838−0655, since none of the spectral data for the hard X-ray emissions from the pulsar have been published.

PSRs	P (ms)	L_{sd} (10^{36} erg s^{-1})	B_s (10^{12} G)	D (kpc)	α (degree)	β (degree)	f_{gap}
B1509−58	151	17	15	4.4	30	15	0.3
J1617−5055	69	16	3.1	6.5	15	25	0.21
J1811−1925	65	6.4	1.7	5	10	35	0.2
J1838−0655	65	6.4	1.7	6.6	–	–	–
J1846−0258	326	8.1	48	5.8	10	35	0.5
J1930+1852	136	12	10	5	20	41	0.28

spectrum of the PSR B1509−58. Lin et al. (2009) also proposed that the X-ray emissions from GeV-quiet SGPSR J1838−0655 are produced by the synchrotron radiation of the pairs, which are produced by the magnetic pair-creation process of the inward gamma-rays from the outer gap.

Main purpose of this paper is to apply the model of the inward emissions to other GeV-quiet SGPSRs, since the member of the GeV-quiet SGPSRs is growing and since no previous studies have been discussed the emission mechanisms. In particular, we will apply our model to four GeV-quiet SGPSRs: PSRs J1617−5055, J1811−1925, J1846−0258 and J1930+1852, for which detailed spectral data in 10–100 keV bands were found in the literature. Although no detection of the emissions above 100 keV has been reported, they share some properties of the emissions with PSR B1509−58; for example, (1) their radio emissions are dim or quiet, (2) the pulse profile in X-ray/soft gamma-ray bands is described by a single broad curve, (3) there are no GeV emissions and (4) the broad-band spectral shape suggests the maximum energy flux at MeV energy bands. It is likely therefore that the emission processes of those GeV-quiet SGPSRs are different from the typical gamma-ray pulsars. The spin-down parameters of those SGPSRs are summarized in Table 1.

In the paper, we also analyse the six year *Fermi* data and determine the upper limit flux of the GeV emissions (Section 2), because we could not find any published results. We describe the theoretical model in Section 3 and compare the calculated spectra and light curves in Section 4. A brief summary is presented in Section 5.

2 *FERMI* DATA ANALYSIS

We used the gamma-ray data from the *Fermi*-LAT to search any gamma-ray emissions from the four SGPSRs: PSR J1617−5055, PSR J1811−1925, PSR J1846−0258 and PSR J1930+1852. The data analysis was performed using the *Fermi* Science Tools package (v9r32p5) available from the *Fermi* Science Support Center (FSSC).[2] The data we used here were obtained from the reprocessed *Fermi* Pass 7 data base and the instrumental response function used was the P7REP_SOURCE_V15 version. We used the data in the period starting from 2008-08-04 15:43:37 to 2014-05-30 01:27:16 (UTC). We selected the photons carrying energy between 100 MeV and 100 GeV within 20° × 20° regions of interest (ROI) centred at the positions of the pulsars. To prevent the contamination by the Earth's albedo, the events with zenith angle greater than 100° or rocking angle greater than 52° were filtered.

Binned likelihood analysis was performed using the *gtlike* function. To model the background source contributions, we included all two year *Fermi* Gamma-ray LAT catalogue point sources (Nolan et al. 2012) associated with the extended source templates within 20° from the ROI centre. The spectral parameters for sources greater than 10° from the pulsars were kept fixed to the values defined in the catalogue. For sources between 6° and 10° away from the centre of ROI, only the spectral indices were kept fixed to the catalogue definitions. The Galactic diffuse background (gll_iem_v05.fits) and the isotropic diffuse background (iso_source_v05.txt) were also included in the modelling. All of these background modelling resources are available from the FSSC.

Using the full energy range extracted, 100 MeV–100 GeV, we modelled the four SGPSRs as point sources using the simple power law

$$\frac{\mathrm{d}N}{\mathrm{d}E} = N_0 \left(\frac{E}{E_0}\right)^{-\Gamma}. \quad (1)$$

The spectral energy distributions under 1 GeV were calculated using the modelled power law with all the spectral indices in the model kept fixed to the best-fitting values. Two equally divided energy bins, 100–316 MeV and 316 MeV–1 GeV, were used in this analysis.

Fig. 2 shows four test-statistic (TS) maps created in the 4° × 4° regions centred at the four pulsars with energy ranged from 100 to 316 MeV. The TS values indicated that there is no detection by the *Fermi*-LAT in this energy band at the locations of the SGPSRs. Only upper limits for the emissions under GeV could be determined from the LAT data. The values were tabulated in Table 2. It is noted that a significant source is detected by *Fermi*-LAT above the GeV range at the position of PSR J1617−5055. Fig. 3 shows a TS map of PSR J1617−5055 with energy ranged from 100 MeV to 100 GeV and TS $\simeq$ 100 (10σ) at the central position. This detection was reported by Xing et al. (2014) and identified as the *Fermi* gamma-ray counterpart to the SNR RCW 103.

3 THEORETICAL MODEL

In our model, we suggest that the emissions from the GeV-quiet SGPSRs are produced via synchrotron radiation of the pairs, which are created by the interaction of the inward gamma-rays and the

[2] http://fermi.gsfc.nasa.gov/ssc/data/analysis/software/

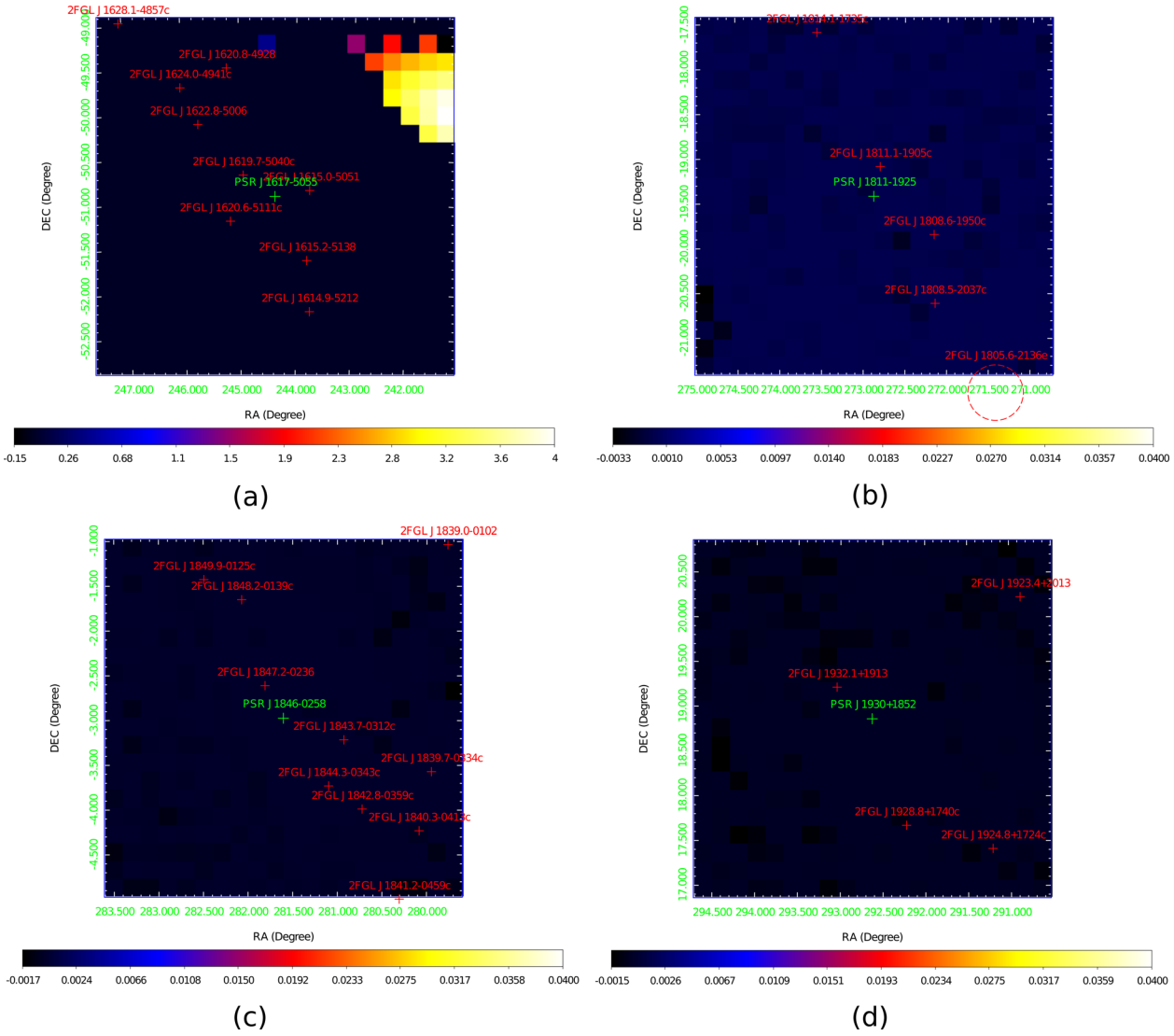

Figure 2. 100–316 MeV TS maps in the $4^\circ \times 4^\circ$ regions centred at (a) PSR J1617−5055, (b) PSR J1811−1925, (c) PSR J1846−0258 and (d) PSR J1930+1852.

Table 2. Upper limits for the pulsars PSR J1617−5055, PSR J1811−1925, PSR J1846−0258 and PSR J1930+1852 in the energy bands: 100–316 MeV and 316 MeV–1 GeV.

PSRs	Emission in 100 MeV–316 MeV (erg cm^{-2} s^{-1})	Emission in 316 MeV–1 GeV (erg cm^{-2} s^{-1})
J1617−5055	$<2.5 \times 10^{-11}$	$<9.1 \times 10^{-12}$
J1811−1925	$<3.7 \times 10^{-12}$	$<4.9 \times 10^{-12}$
J1846−0258	$<4.4 \times 10^{-11}$	$<1.0 \times 10^{-11}$
J1930+1852	$<1.9 \times 10^{-11}$	$<5.7 \times 10^{-12}$

strong magnetic field near the polar cap region. Fig. 4 shows a schematic picture for the inward gamma-ray emissions and subsequent pair-creation process and synchrotron radiation process. We emphasize that the viewing geometry is a crucial factor to differentiate between the typical gamma-ray pulsars and SGPSRs. Our model expects that a *millisecond* pulsar does not show a GeV-quiet soft gamma-ray spectrum, since its dipole magnetic field $B_s \sim 10^{8\text{–}9}$ G is too small to operate the magnetic pair-creation process (except for very close to stellar surface, where the stronger multipole magnetic field may dominate the dipole field). Since a detailed method of the calculation was described by Wang et al. (2013), we briefly mention the guideline of the model.

3.1 Inward emissions of the outer gap

In the outer gap model, the charged particles are accelerated by the electric field parallel to the magnetic field, and emit the GeV gamma-rays via the curvature radiation process. Takata, Chang &

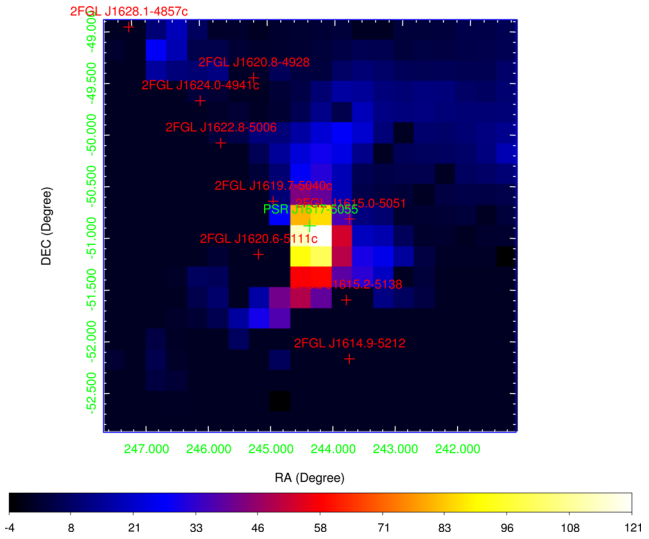

Figure 3. TS map for PSR J1617−5055 in the energy range from 100 MeV to 100 GeV.

Shibata (2008) argued that the outer gap accelerator produces *outward* and *inward* gamma-rays, which are produced by the outgoing particles and incoming particles accelerated in the gap; for the magnetic inclination angle smaller than 90°, the outgoing and incoming particles are positrons and electrons, respectively. In the outer gap, since (i) the strong acceleration region extends between the null charge surface of the Goldreich–Julian charge density and the light cylinder and (ii) most of pairs are produced *around the null charge surface* (Cheng, Ruderman & Zhang 2000), the outgoing particles are accelerated by almost full potential drop in the gap, while the incoming particles feel only potential drop between the inner boundary and the pair-creation position. Hence, it is expected that the luminosity of the outward propagating gamma-rays is about one order of magnitude larger than that of inward propagating gamma-rays, suggesting the *Fermi* has preferentially detected the outward emissions of the outer gap. Within the framework of the outer gap model, the gamma-ray luminosity can be written as

$$L_\gamma \sim I_{\rm gap} V_{\rm gap}, \tag{2}$$

where $I_{\rm gap}$ is the total current in the outer gap and $V_{\rm gap}$ is electric potential drop along the magnetic field line. As aforementioned, in the pair-creation region in the outer gap accelerator, the outgoing particles are accelerated by almost full potential drop in the gap, which can be estimated as

$$V_{\rm gap}^{\rm out} \sim f_{\rm gap}^2 B_{\rm lc} R_{\rm lc}, \tag{3}$$

where $R_{\rm lc} = Pc/2\pi$ is the light cylinder radius, $B_{\rm lc}$ is the magnetic field at the light cylinder and $f_{\rm gap}$, which takes a value of ∼0.2–0.3, is the ratio of the gap thickness to the light cylinder radius at the light cylinder. For the inward emissions, the incoming particles are accelerated with a potential of $V_{\rm gap}^{\rm in} \sim 0.1 V_{\rm gap}^{\rm out}$.

In the outer gap magnetosphere, the charge particles are accelerated by the electric field along the magnetic field line $E_{||} \sim V_{\rm gap}/R_{\rm lc}$ and emit gamma-rays through the curvature radiation process. Assuming balance between the electric force and radiation drag force, the saturated Lorentz factor is proportional to $\Gamma \propto V_{\rm gap}^{1/4}$. As a result, the typical energy of the curvature radiation is proportional to $E_{\rm c} \propto \Gamma^3 \propto V_{\rm gap}^{3/4}$. Since $V_{\rm gap}^{\rm in} \sim 0.1 V_{\rm gap}^{\rm out}$, the energy of the curvature radiation of inward emissions is a factor of ∼5 smaller than that of the outward emissions and it typically becomes 0.1–1 GeV.

For the outer gap accelerator, the strong acceleration region extends beyond the null charge surface, which is defined by surface of $\Omega \cdot B = 0$. It has been proposed that the active outer gap with the electric current can be extended 'below' null charge surface (Hirotani 2006; Takata et al. 2006), but the accelerating electric field below the null charge surface is significantly reduced by the electron and positron pairs with a very weak field. We approximate the electric structure below the null charge surface as

$$E_{||}(r < r_{\rm null}) = \frac{(r/r_{\rm in})^2 - 1}{(r_{\rm null}/r_{\rm in})^2 - 1} E_{||,{\rm null}}, \tag{4}$$

where $E_{||,{\rm null}}$ is the electric field strength at the null charge surface and is given by our three-dimensional two-layer structure model (Wang et al. 2010) and $r_{\rm null}$ is the radial distance to the null charge surface, which is a function of the inclination angle and azimuth angle. In addition, $r_{\rm in}$ is the radial distance to the inner boundary of the outer gap and is set at 20 stellar radii.

Near and below the inner boundary, the incoming particles lose their energy via the curvature radiation process. When the Lorentz factor of the incoming particles drops low enough, the curvature energy loss time-scale becomes comparable to the time-scale of the particle's movement to the stellar surface. In such a case, we can show that the energy of the curvature photon is $9 m_{\rm e} c^2/8\alpha_{\rm f} \sim 100$ MeV, where α is the fine structure constant

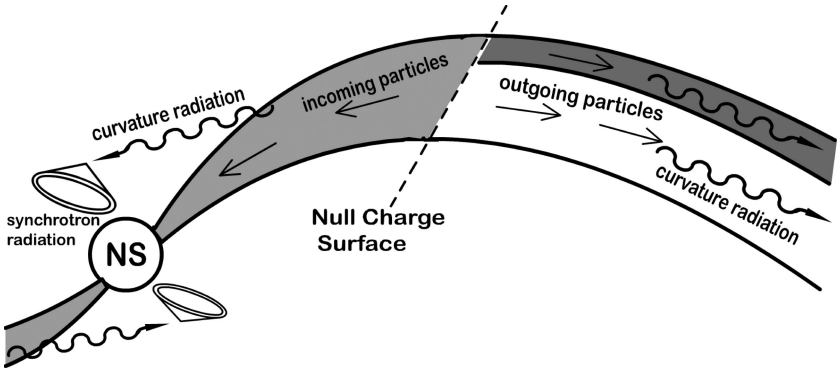

Figure 4. Schematic view of the inward emissions from the outer gap accelerator. This figure is from Wang et al. (2013). Primary particles accelerated in the gap emit the gamma-ray photons via the curvature radiation process in the direction of its motion, which comprises the motion along the magnetic field line and the corotation motion. Incoming particles emit the 100 MeV–1 GeV gamma-rays below the null charge surface. The 100 MeV–1 GeV gamma-rays emitted near the stellar surface interact with the strong magnetic field and produce new pairs. The gyration motion of the pairs with an infinite pitch angle produces hard X-ray/soft gamma-rays via the synchrotron radiation, which covers a wider sky area than the curvature radiation of the primary particles.

(Takata et al. 2010). Hence, we expect that the incoming particles emit 0.1–1 GeV photons between the null charge surface and the stellar surface. The gamma-ray photons emitted below the null charge surface may pass through the strong magnetic field region near the stellar surface and may initiate magnetic pair-creation cascade.

3.2 Magnetic pair-creation cascade

The typical cut-off energy (0.1–1 GeV) in the spectrum of the inward emissions will be still higher than the spectral cut-off energy (∼1–10 MeV) of the GeV-quiet SGPSRs; for example, the original SGPSR, PSR B1509−58, shows a spectral cut-off at ∼5 MeV. To explain the position of the spectral cut-off of PSR B1509−58, we simulate the pair-creation cascades of the inward gamma-ray emissions (Wang et al. 2013). If the inward-propagating gamma-rays emitted below the null charge surface pass through near the stellar surface, they may be absorbed by the magnetic field and be converted into electron and positron pairs (magnetic pair-creation process). The mean free path of the magnetic pair creation may be written as (Erber 1966)

$$\ell = \frac{4.4}{(e^2/\hbar c)}\frac{\hbar}{m_{\rm e}c}\frac{B_{\rm c}}{B_\perp}\exp\left(\frac{4}{3\chi}\right), \tag{5}$$

where $\chi = \hbar\omega B_\perp/(2m_{\rm e}c^2B_{\rm c})$ and $B_\perp = B\sin\theta_{\rm p}$ with $\theta_{\rm p}$ being the angle between the magnetic field direction and propagating direction of the photon and $B_{\rm c} = 4.4\times10^{13}$ G. We calculate the optical depth $\tau_{\rm opt}(s_i) = \int_{s_{i-1}}^{s_i} {\rm d}s/\ell(s) (i = 1, 2, 3, \ldots)$, where $s_0 = 0$ corresponds to the position of the emitted point. We determine the pair-creation position s_i from the condition $\tau(s_{i+1}) - \tau(s_i) = 0.1$ and calculate the number of created pairs from the equation $\delta N(s_i) = N_0\{\exp[-\tau(s_{i-1})] - \exp[-\tau(s_i)]\}$, where N_0 is the emitted gamma-rays in the gap. We have also taken into account the pair-creation process of the gamma-rays with the X-rays.

3.3 Synchrotron emissions from new pairs

The created pairs have a pitch angle $\theta_{\rm p}$ and lose their energy via the synchrotron radiation. We solve the evolution of the Lorentz factor (γ) of the pairs with the equations of

$$\frac{{\rm d}P_{||}}{{\rm d}t} = -\frac{2e^4B^2\gamma^2\sin^2\theta_{\rm p}}{3m^2c^4}\cos\theta_{\rm p} \tag{6}$$

and

$$\frac{{\rm d}P_\perp}{{\rm d}t} = -\frac{2e^4B^2\gamma^2\sin^2\theta_{\rm p}}{3m^2c^4}\sin\theta_{\rm p}, \tag{7}$$

where $P_{||} = m_{\rm e}c\gamma\cos\theta_{\rm p}$ and $P_\perp = m_{\rm e}c\gamma\sin\theta_{\rm p}$. Since the magnetic field and Lorentz factor of the particle at the pair-creation position are $B_\perp = 2m_{\rm e}c^2B_{\rm c}/(\chi E_\gamma)$ and $\gamma = E_\gamma/2m_{\rm e}c^2$, respectively, the maximum energy of the synchrotron radiation of the new born pairs becomes as

$$E_{\rm syn,max} \sim \frac{3\hbar\gamma^2eB_\perp}{2m_{\rm e}c} \sim \frac{3E_\gamma}{4\chi} \sim 38\left(\frac{E_\gamma}{0.5\,{\rm GeV}}\right)\left(\frac{\chi}{0.1}\right)^{-1}{\rm MeV}, \tag{8}$$

suggesting that the spectrum of the synchrotron radiations of the pairs, which are produced by the magnetic pair-creation process, has a spectral turnover around 10 MeV. The position of this spectral turnover can explain that of the GeV-quiet SGPSRs. Therefore, we suggest that the observed high-energy emissions from GeV-quiet SGPSRs are produced through the synchrotron radiation occurred near the stellar surface. We also take into account the magnetic pair-creation process of the synchrotron photons, which was ignored in Wang et al. (2013).

We take into account the effects of the pitch angle and the gyration motion on the emission direction of synchrotron radiation. The particle motion is expressed by the sum of the motion along the magnetic field line, gyration motion and corotation motion. Taking the z-axis along the rotation axis, the particle motion is calculated from (Takata, Chang & Cheng 2007; Wang et al. 2013)

$$\boldsymbol{v} = \lambda v_{\rm p}\boldsymbol{v}'_{\rm syn}/|\boldsymbol{v}'_{\rm syn}| + \boldsymbol{\Omega}\times\boldsymbol{r}, \tag{9}$$

where $v_{\rm p}$ is calculated from the condition $|\boldsymbol{v}| = c$ and $\boldsymbol{v}'_{\rm syn}$ is given by

$$\begin{aligned} v'_{\rm syn,x} &= \hat{B}_x + \tan\theta_{\rm p}(u_x\cos T + v_x\sin T)\\ v'_{\rm syn,y} &= \hat{B}_y + \tan\theta_{\rm p}(u_y\cos T + v_y\sin T),\\ v'_{\rm syn,z} &= \hat{B}_z + \tan\theta_{\rm p}(u_z\cos T + v_z\sin T) \end{aligned} \tag{10}$$

where $\theta_{\rm p}$ is the pitch angle of the created pairs and T is the phase of the gyration motion. In the equation above, $\hat{\boldsymbol{B}} = \boldsymbol{B}/|B|$, $\boldsymbol{u} = [B_y/(B_x^2+B_y^2)]^{1/2}, -B_x/(B_x^2+B_y^2)^{1/2}, 0)$ and $\boldsymbol{v} = (\boldsymbol{B}\times\boldsymbol{u})/|\boldsymbol{B}\times\boldsymbol{u}|$. In addition, λ represents the direction of the particle motion projected to the magnetic field line; $\lambda = 1$ for $\theta_{\rm p} \le 90^\circ$ and $\lambda = -1$ for $\theta_{\rm p} > 90^\circ$.

The Earth viewing angle (β) measured from the rotation axis and the pulse phase ψ for a synchrotron (or curvature) photon can be calculated from

$$\cos\beta = \frac{v_z}{\boldsymbol{v}} \tag{11}$$

and

$$\psi = -\cos^{-1}(v_x/\sqrt{v_x^2+v_y^2}) - \frac{\boldsymbol{r}\cdot\boldsymbol{v}}{vR_{\rm lc}}, \tag{12}$$

respectively, where $\boldsymbol{r}$ is the vector to the radiation point. For each viewing angle β, we calculate the phase-averaged spectrum and compare the result with the observations (Section 4).

The synchrotron emissions from the pairs ($\theta_{\rm p} \neq 0$) with the gyration motion cover a wider sky area than the curvature radiation of the primary particles ($\theta_{\rm p} = 0$), which is emitted along the magnetic field line. Wang et al. (2013) discussed the evolution of the X-ray/gamma-ray spectrum for the different viewing geometry. Fixing magnetic inclination angle at $\alpha = 20^\circ$, the *outward curvature emissions* dominate the inward emissions and the spectrum extends up to several GeV if the viewing angle is $\beta \sim 70^\circ$–90°. For mildly viewing angle $\beta \sim 50^\circ$, the inward curvature emissions and subsequent synchrotron radiation of the pairs can contribute to the spectrum. For small inclination angle $\beta \sim \alpha$ or $\beta < \alpha$, only synchrotron radiation of the pairs created by the magnetic pair creation contributes to the observations, and the spectral peak in νF_ν appears at around ∼1 MeV, which can explain the spectral properties of GeV-quiet SGPSRs. Hence, our model suggests that the GeV-quiet SGPSR is a peculiar case of the viewing geometry and it has a relatively small viewing angle and inclination angle comparing with the normal gamma-ray pulsars.

In the present calculation, we apply the rotating dipole magnetic field in vacuum (Cheng et al. 2000). Force-free magnetosphere has been investigated for magnetic field and current structure in the pulsar magnetosphere (Contopoulos, Kazanas & Fendt 1999; Spitkovsky 2006), and provides a distinct GeV pulse profile from the vacuum dipole field (Bai & Spitkovsky 2010). More realistic pulsar magnetosphere will be between the vacuum dipole field and the fore-free field (e.g. Kalapotharakos et al. 2012; Li, Spitkovsky

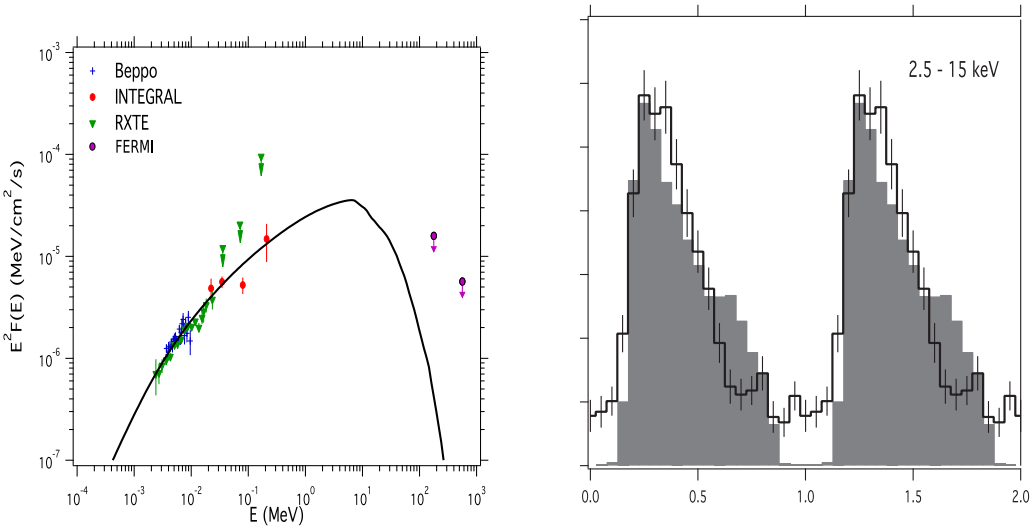

Figure 5. The spectrum (left) and X-ray light curve of PSR J1617−5055. The solid line in the left-hand panel and the grey histogram in the right-hand panel show the calculated spectrum and the light curve, respectively. The results are for the inclination angle of $\alpha = 15^\circ$ and the Earth viewing angle of $\beta = 25^\circ$. For the observed flux, the data were taken from Landie et al. (2007) for *BeppoSAX* and *INTEGRAL* and from Kuiper & Hermsen (in preparation) for *RXTE*. The upper limit of *Fermi* data was determined by this study. For the light curve, the data were taken from Becker & Aschenbach (2002).

& Tchekhovskoy 2012). In the present calculation, however, since the emission regions in X-ray/soft gamma-ray bands are near the neutron star surface, where the force-free field and vacuum dipole field may be close to each other, the rotating vacuum dipole field may provide a good approximation to discuss the pulse profile.

4 RESULTS

To fit the observed spectrum, main model parameters are the fractional gap thickness $f_{\rm gap}$, the magnetic inclination angle α and the Earth viewing angle β. The inclination angle and the viewing angle of a pulsar are sometimes constrained by a rotating vector model, which fits the observations of the radio polarization (Radhakrishnan & Cooke 1969). For instance, the fitting of the original SGPSR, PSR B1509−58, suggests the inclination angle of $\alpha < 60^\circ$ (Crawford et al. 2001). The geometrical model of the pulsar wind nebula (PWN) is also used to constrain the viewing geometry of the pulsar (Gaensler et al. 2002; Ng & Romani 2008). Using *Chandra* data, for example, Lu et al. (2002) found clear torus structure of the PWN surrounding the SGPSR PSR B1930+1852 and suggested the Earth viewing angle of $\beta = 41^\circ$. We emphasize that within the framework of our model, the viewing geometry that explains (1) the softness of the spectra, (2) its flux level and (3) the single peak in the light curve of the GeV-quiet SGPSRs is constrained in a narrow range of the parameters. In Table 1, we tabulate the best-fitting parameters of the inclination angle and the Earth viewing angle for four GeV-quiet SGPSRs.

4.1 J1617−5055

The 69 ms spin-down powered pulsar PSR J1617−5055 was discovered by the X-ray observations (Torii et al. 1998; Garmire et al. 1999; Becker & Aschenbach 2002; Kargaltsev, Pavlov & Wong 2009) with the radio pulsation founded shortly afterwards (Kaspi et al. 1998). Soft gamma-ray emissions at ∼100 keV bands were discovered by *INTEGRAL* (Landi et al. 2007). The timing analyses show that the spin-down dipole magnetic field is $B_{\rm s} \sim 3 \times 10^{13}$ G and the characteristic age is $\tau_{\rm a} \sim 8.1$ kyr. The dispersion measure gives the distance to the pulsar of $d \sim 6.1$–6.9 kpc. The X-ray spectrum below ∼10 keV is fitted by a single power-law function with a photon index of $p \sim 1.4$, and there is a spectral break around 10 keV (Torii et al. 1998; Becker & Aschenbach 2002). The inferred X-ray conversion efficiency in 0.5–10 keV bands is $L_{\rm X}/\dot{E} \sim 1.4 \times 10^{-3}$ for a distance of $d = 6$ kpc (Becker & Aschenbach 2002). These X-ray properties are common among the GeV-quiet SGPSR. Both the X-ray and radio pule profiles of PSR J1617−5055 show a single peak, but absolute phase difference between the X-ray and radio peaks has not been known.

Fig. 5 compares the calculated spectrum (left-hand panel, solid line) and X-ray light curve (right-hand panel, grey histogram) with the observations; the phase 0 (and 0.5) in Fig. 5 corresponds to the phase at which the magnetic axis points towards the Earth. We assumed the inclination angle of $\alpha = 15^\circ$ and the Earth viewing angle measured from the rotation axis of $\beta = 25^\circ$. In the present scenario, we have argued that the emissions from the GeV-quiet SGPSRs are created by the synchrotron radiation process of the pairs, which are produced by the interaction of the inwardly emitted GeV gamma-rays and the strong magnetic field near the pulsar. Since the pairs are mainly produced above the polar cap, the pulse peak with a strong synchrotron emission appears if the line of sight cuts near the polar cap region. Hence, the condition that the earth viewing angle is not significantly shifted from the magnetic inclination angle is required. Furthermore, a small inclination angle is required to avoid the detection of curvature radiation (GeV emissions) from the outer gap.

4.2 J1811−1925

The 65 ms pulsar PSR J1811−1925 at the centre of G11.2−0.3 was discovered by *ASCA* observations (Torii et al. 1997; Kaspi et al. 2001). This pulsar has not been detected in the radio band (Crawford et al. 1998). The X-ray timing analysis suggests that the spin-down dipole magnetic field is $B_{\rm s} \sim 2 \times 10^{12}$ G and spin-down age is $\tau \sim 24$ kyr (Torii et al. 1999). However, the *Chandra* observation combined with Very Large Array observations (Roberts et al. 2003) suggests that the reverse shock of SNR has not yet

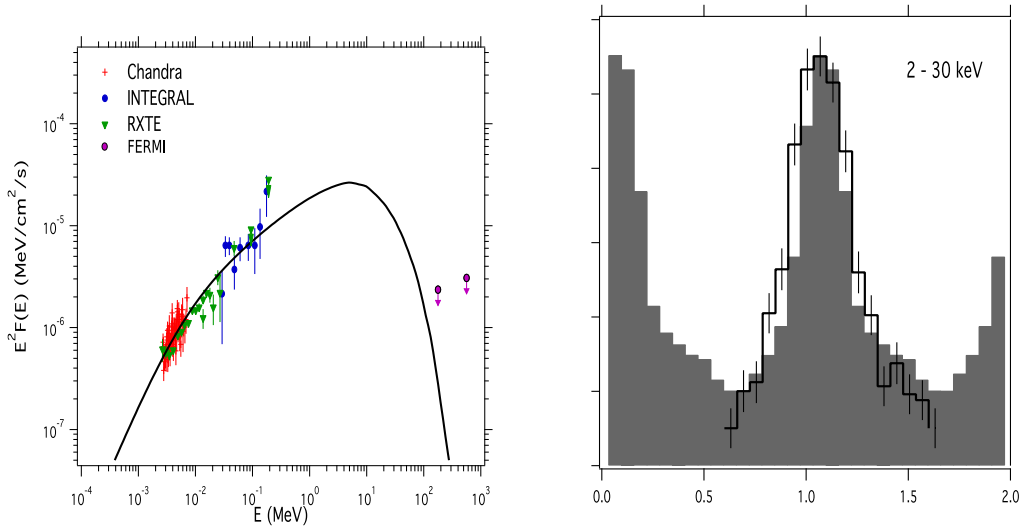

Figure 6. Same as with Fig. 5, but for PSR J1811−1925. The model calculation is result for $\alpha = 10^\circ$ and $\beta = 35^\circ$, respectively. For the observed flux, the data were taken from Dean et al. (2008) for *Chandra* and *INTEGRAL* and from Kuiper & Hermsen (in preparation) for *RXTE*. For the light curve, the data were taken from Gavriil, Kaspi & Roberts (2004). Although the pulsed component above 10 keV was not discussed in Dean et al. (2008), it may dominate the nebula component above 10 keV (cf. fig. 2 in Dean et al. 2008).

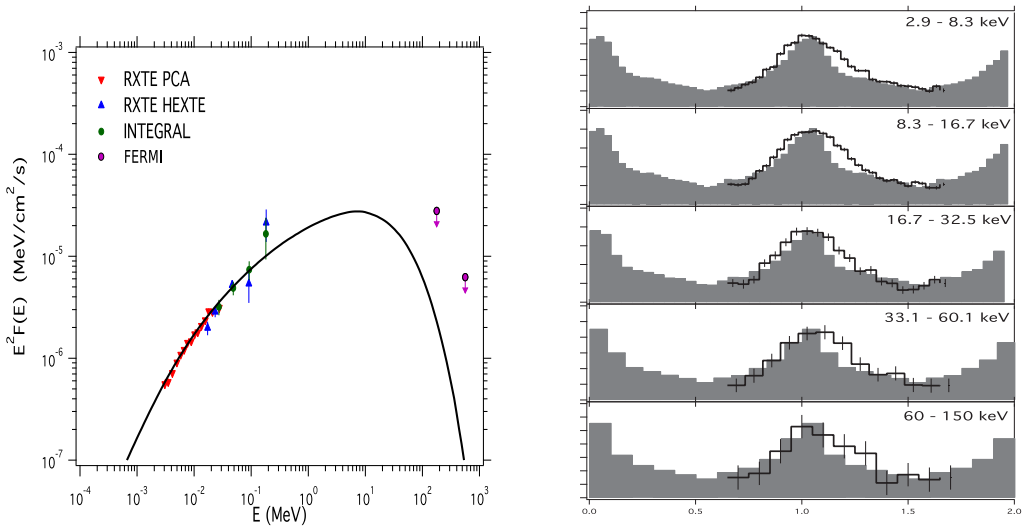

Figure 7. Same as with Fig. 5, but for PSR J1846−0258. The model calculation is result for $\alpha = 10^\circ$ and $\beta = 35^\circ$, respectively. For the observed flux and light curve in X-ray/soft gamma-ray bands, the data were taken from Kuiper & Hermsen (in preparation).

reached the PWN, which indicates that the system is about 2000 yr old, which is consistent with the historical record of supernova in AD 386 (Clark & Stephenson 1977). The distance to the pulsar is $d \sim 5$ kpc as inferred from H I measurements (Becker, Markert & Donahue 1985; Green et al. 1988). Fig. 6 compares the calculated spectrum (left-hand panel, solid line) and X-ray light curve (right-hand panel, grey histogram) with the observations. We assumed the inclination angle of $\alpha = 10^\circ$ and the Earth viewing angle measured from the rotation axis of $\beta = 35^\circ$.

4.3 J1846−0258

The 326 ms pulsar PSR J1846−0258 (also known as AX J1846.4−0258) was discovered by Gotthelf et al. (2000) in the X-ray bands, and is at the centre of SNR Kes 75 (cf. Kesteven 1968; Helfand, Collins & Gotthelf 2003; Molkov et al. 2004; Bird et al. 2007; Kumar & Safi-Harb 2008; McBride et al. 2008; Ng et al. 2008). No radio emission has been observed from PSR J1846−0258 (Archibald et al. 2008), but the X-ray timing analysis reveals the surface dipole magnetic field of $B_s \sim 4.8 \times 10^{13}$ G and the characteristic age of $\tau \sim 728$ yr. It is thought that PSR 18460−258 is a transition object between rotation-powered pulsar and magnetically powered pulsar (i.e. *magnetar*). In fact, the pulsar showed a magnetar-like X-ray outburst accompanied by a large glitch in 2006 (Gavriil et al. 2008).

Parent et al. (2011) derived the upper limit of the pulsed gamma-ray flux at 3×10^{-11} erg cm^{-2} s^{-1}, which will be consistent with the result of our *Fermi* data analysis (cf. Table 2 and Fig. 7). The distance to the pulsar is the controversial in the range of $d = 5$–19 kpc (Becker & Helfand 1984; Leahy & Tian 2008; Su et al. 2009). It is also known that the pulsar is embedded in a PWN (Helfand et al. 2003; McBride et al. 2008). Modelling of the torus

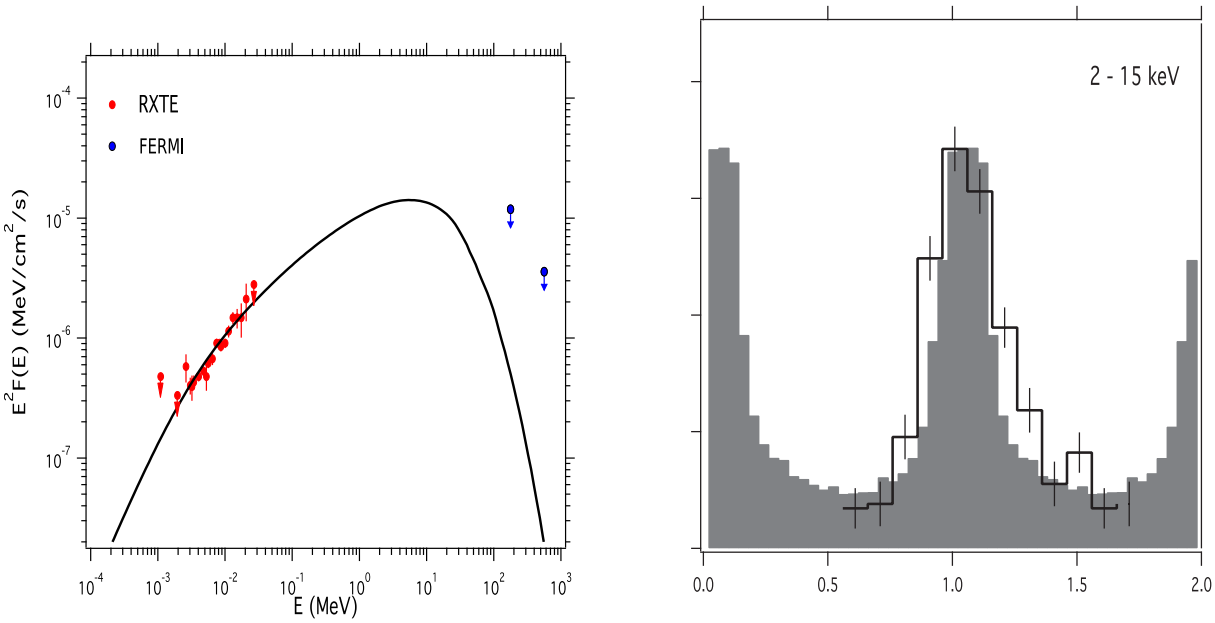

Figure 8. Same as with Fig. 5, but for PSR J1930+1852. The model calculation is result for $\alpha = 20^\circ$ and $\beta = 41^\circ$, respectively. The data were taken from Kuiper & Hermsen (in preparation) for observed X-ray flux and from Lu et al. (2007) for the X-ray light curve.

in the PWN suggests a line-of-sight angle $\beta \sim 60^\circ$ (Ng & Romani 2008). In our model, on the other hand, we require a smaller viewing angle $\beta \sim 35^\circ$ with $\alpha \sim 10^\circ$ to reproduce the observed emission properties.

Fig. 7 compares the calculated spectrum (left-hand panel, solid line) and X-ray light curve (right-hand panel, grey histogram) with the observations. In the figure, we show the light curves in the different energy bands. The observations suggest a single broad peak in X-ray/soft gamma-ray bands, which can be explained by the present model.

4.4 J1930+1852

The 136 ms radio pulsar PSR J1930+1852 was found in SNR G54.1+0.3 by Camilo et al. (2002). Both the X-ray and radio pule profiles of PSR J1930+1852 show a single peak, but absolute phase difference between the X-ray and radio peaks has not been known. The timing analyses show that the spin-down age of this pulsar is 2.9 kyr, and the surface dipole magnetic field is $B_s \sim 1 \times 10^{13}$ G. Lu et al. (2002) suggested that the distance of SNR G54.1+0.3 is about $d \sim 5$ kpc by measuring the X-ray absorption column density. PSR J1930+1852 is surrounded by a PWN, which has clear torus and jet structure. The ratio between the observed semimajor and semiminor axes of the torus of PWN suggests that the Earth viewing angle inferred from the geometrical model is $\beta \sim 41^\circ$ (Lu et al. 2002), which is used in the calculation. Fig. 8 compares the calculated spectrum (left-hand panel, solid line) and X-ray light curve (right-hand panel, grey histogram) with the observations. We assumed the inclination angle of $\alpha = 20^\circ$ and the Earth viewing angle measured from the rotation axis of $\beta = 41^\circ$.

5 DISCUSSION AND SUMMARY

The present model suggests that the observed X-ray/soft gamma-rays are the synchrotron emissions from the high magnetic field region near the stellar surface, and the difference between the magnetic inclination angle and the Earth viewing angle is small, say $|\alpha - \beta| \leq 30^\circ$. To avoid the GeV emissions from the outer gap, furthermore, the inclination angle is required to be small, say $\alpha \leq 30^\circ$. We emphasize that the GeV-quit SGPSRs actually emit outgoing GeV gamma-rays from the outer gap, which make gamma-ray spectra of *Fermi*-LAT pulsars, but our line of sight is out of emission cone due to the smaller magnetic inclination and a smaller Earth viewing angle. For the Earth viewing angleof $\beta \sim 40^\circ$–50°, the synchrotron emissions from the incoming pairs and the GeV emissions of outgoing particles can be observed, as we described in Section 3. This may be the case for GeV-loud SGPSRs PSRs J0205+6449 and J2229+6114, which show a very soft GeV spectrum and the smaller ratio of the GeV fluxes to X-ray fluxes comparing with the typical gamma-ray pulsars (e.g. Vela pulsar; Kuiper & Hermsen 2013). For the viewing angle of $\beta \sim 70^\circ$–90°, the outward GeV emissions make a spectral peak in νF_ν at several GeV. Within the framework of our scenario, therefore, the viewing geometry is a crucial factor to discriminate between the normal gamma-ray pulsars and SGPSRs, and the GeV-quiet SGPSR is peculiar case of the viewing geometry.

The GeV-quiet SGPSRs are relatively young and have higher spin-down powers compared with *Fermi*-LAT pulsars, as shown in Fig. 1; the typical characteristic age and the spin-down power of the GeV-quiet SGPSRs are $\tau_s \sim 10^{3-4}$ yr and $L_{sd} \sim 0.5$–1×10^{37} erg s^{-1}. With the current study, the reason why GeV-quiet SGPSRs with the characteristic age of $\tau_s > 10^4$ yr and $L_{sd} < 5 \times 10^{36}$ erg s^{-1} have not yet found, while many typical gamma-ray pulsars with those spin-down parameters have been found by the *Fermi* is not obvious. However, we expect that with the appropriate viewing geometry, the pulsars with higher surface magnetic field and/or high-spin-down pulsars are preferentially detected as the GeV-quiet SGPSRs. For the future study, therefore, we will study the evolution of spectrum in X-ray/gamma-ray bands with the viewing geometry, spin-down parameters, etc. and will discuss the population of the GeV-quiet SGPSR, GeV-loud SGPSRs and typical gamma-ray pulsars. The

linking among these three groups of the gamma-ray pulsars will provide us a comprehensive picture of the high-energy pulsars.

ACKNOWLEDGEMENTS

We thank Drs L. Kuiper and W. Hermsen for useful discussion and for providing us the X-ray/soft gamma-ray data. We express our appreciation to an anonymous referee for useful comments. This work is partially supported by a 2014 GRF grant of Hong Kong Government under HKU 17300814P and Seed Funding Programme for Basic Research under HKU 2012-7159004 and 201310159026.

REFERENCES

Abdo A. A. et al., 2010a, ApJ, 713, 154
Abdo A. A. et al., 2010b, ApJ, 714, 936
Abdo A. A. et al., 2013, ApJS, 208, 17
Aliu E. et al., 2008, Science, 322, 1221
Archibald A. M., Kaspi V. M., Livingstone M. A., McLaughlin M. A., 2008, ApJ, 688, 550
Bai X.-N., Spitkovsky A., 2010, ApJ, 715, 1282
Becker W., Aschenbach B., 2002, in Becker W., Lesch H., Trümper J., eds, Proc. Vol. 270, WE-Heraeus Seminar on Neutron Stars, Pulsars, and Supernova Remnants. MPE Report 278. Max-Plank-Institut für extraterrestrische Physik, Garching bei München, p. 64
Becker R. H., Helfand D. J., 1984, ApJ, 283, 154
Becker R. H., Markert T., Donahue M., 1985, ApJ, 296, 461
Bird A. J. et al., 2007, ApJS, 170, 175
Camilo F., Lorimer D. R., Bhat N. D. R., Gotthelf E. V., Halpern J. P., Wang Q. D., Lu F. J., Mirabal N., 2002, ApJ, 574, L71
Cheng K. S., Ruderman M., Zhang L., 2000, ApJ, 537, 964
Clark D. H., Stephenson F. R., 1977, The Historical Supernovae. Pergamon Press, Oxford
Contopoulos I., Kazanas D., Fendt C., 1999, ApJ, 511, 351
Crawford F., Kaspi V. M., Manchester R. N., Camilo F., Lyne A. G., D'Amico N., 1998, Mem. Soc. Astron. Ital., 69, 951
Crawford F., Kaspi V. M., Manchester R. N., Camilo F., Lyne A. G., D'Amico N., 2001, Mem. Soc. Astron. Ital., 69, 951
Dean A. J. et al., 2008, MNRAS, 384, L29
Erber T., 1966, Rev. Mod. Phys., 38, 626
Gaensler B. M., Arons J., Kaspi V. M., Pivovaroff M. J., Kawai N., Tamura K., 2002, ApJ, 569, 878
Garmire G. P., Garmire A. B., Burrows D. N., Pavlov G., 1999, Am. Astron. Soc., 195, 3913
Gavriil F. P., Kaspi V. M., Roberts M. S. E., 2004, Adv. Space Res., 33, 592
Gavriil F. P., Gonzalez M. E., Gotthelf E. V., Kaspi V. M., Livingstone M. A., Woods P. M., 2008, Science, 219, 1802
Gotthelf E. V., Vasisht G., Boylan-Kolchin M., Torii K., 2000, ApJ, 542, L37
Green D. A., Gull S. F., Tan S. M., Simon A. J. B., 1988, MNRAS, 231, 735
Harding A. K., Baring M. G., Gonthier P. L., 1997, ApJ, 476, 246
Helfand D. J., Collins B. F., Gotthelf E. V., 2003, ApJ, 582, 783
Hirotani K., 2006, ApJ, 652, 1475
Kalapotharakos C., Harding A. K., Kazanas D., Contopoulos I., 2012, ApJ, 754, L7
Kargaltsev O., Pavlov G. G., Wong J. A., 2009, ApJ, 690, 891
Kaspi V. M., Crawford F., Manchester R. N., Lyne A. G., Camilo F., D'Amico N., Gaensler B. M., 1998, ApJ, 503, L161
Kaspi V. M., Roberts M. E., Vasisht G., Gotthelf E. V., Pivovaroff M., Kawai N., 2001, ApJ, 560, 371
Kesteven M. J. L., 1968, Aust. J. Phys., 21, 739
Kuiper L., Hermsen W., 2013, The Fast and the Furious: Energetic Phenomena in Isolated Neutron Stars, Pulsar Wind Nebulae and Supernova Remnants in Madrid, Spain, available at: http://xmm.esac.esa.int/external/xmm_science/workshops/2013_science/
Kuiper L., Hermsen W., Cusumano G., Diehl R., Schönfelder V., Strong A., Bennett K., McConnell M. L., 2001, A&A, 378, 918
Kumar H. S., Safi-Harb S., 2008, ApJ, 678, L43
Landi R., de Rosa A., Dean A. J., Bassani L., Ubertini P., Bird A. J., 2007, MNRAS, 380, 926
Leahy D. A., Tian W. W., 2008, A&A, 280, L25
Li J., Spitkovsky A., Tchekhovskoy A., 2012, ApJ, 746, L60
Lin L. C.-C., Takata J., Hwang C.-Y., Liang J.-S., 2009, MNRAS, 400, 168
Lu F. J., Wang Q. D., Aschenbach B., Durouchoux P., Song L. M., 2002, ApJ, 568, L49
Lu F., Wang Q. D., Gotthelf E. V., Qu J., 2007, ApJ, 663, 315
Manchester R. N., Hobbs G. B., Teoh A., Hobbs M., 2005, AJ, 129, 1993
McBride V. A. et al., 2008, A&A, 477, 249
Molkov S. V., Cherepashchuk A. M., Lutovinov A. A., Revnivtsev M. G., Postnov K. A., Sunyaev R. A., 2004, Astron. Lett., 30, 534
Ng C.-Y., Romani R. W., 2008, ApJ, 673, 411
Ng C.-Y., Slane P. O., Gaensler B. M., Hughes J. P., 2008, ApJ, 686, 508
Nolan P. L. et al., 2012, ApJS, 199, 31
Parent D. et al., 2011, ApJ, 743, 170
Radhakrishnan V., Cooke D. J., 1969, Astrophys. Lett., 3, 225
Roberts M. S. E., Tam C. R., Kaspi V. M., Lyutikov M., Vasisht G., Pivovaroff M., Gotthelf E. V., Kawai N., 2003, ApJ, 588, 992
Spitkovsky A., 2006, ApJ, 648, L51
Su Y., Chen Y., Yang J., Koo B., Zhou X., Jeong I., Zhang C., 2009, ApJ, 694, 376
Takata J., Shibata S., Hirotani K., Chang H.-K., 2006, MNRAS, 366, 1310
Takata J., Chang H.-K., Cheng K. S., 2007, ApJ, 656, 1044
Takata J., Chang H.-K., Shibata S., 2008, MNRAS, 386, 748
Takata J., Wang Y., Cheng K. S., 2010, ApJ, 715, 1318
Torii K., Tsunemi H., Dotani T., Mitsuda K., 1997, ApJ, 489, L145
Torii K. et al., 1998, ApJ, 494, L207
Torii K., Tsunemi H., Dotani T., Mitsuda K., Kawai, Kinugasa K., Saito Y., Shibata S., 1999, ApJ, 523, L69
Ulmer M. P. et al., 1993, ApJ, 417, 738
Wang Y., Takata J., Cheng K. S., 2010, ApJ, 720, 178
Wang Y., Takata J., Cheng K. S., 2013, ApJ, 764, 51
Xing Y., Wang Z., Zhan X., Chen Y., 2014, ApJ, 781, 64
Zhang L., Cheng K. S., 2000, A&A, 363, 575

This paper has been typeset from a TEX/LATEX file prepared by the author.